Pulsar searches of Fermi unassociated sources with the Effelsberg telescope

E. D. Barr, Lucas Guillemot, D. J. Champion, M. Kramer, R. P. Eatough, K. J. Lee, J. P. W. Verbiest, C. G. Bassa, F. Camilo, Ö. Çelik, et al.

Monthly Notices
of the
ROYAL ASTRONOMICAL SOCIETY

MNRAS **429,** 1633–1642 (2013) doi:10.1093/mnras/sts449

Pulsar searches of *Fermi* unassociated sources with the Effelsberg telescope

E. D. Barr,[1⋆] L. Guillemot,[1⋆] D. J. Champion,[1] M. Kramer,[1,2] R. P. Eatough,[1] K. J. Lee,[1] J. P. W. Verbiest,[1] C. G. Bassa,[2] F. Camilo,[3,4] Ö. Çelik,[5,6,7] I. Cognard,[8,9] E. C. Ferrara,[5] P. C. C. Freire,[1] G. H. Janssen,[2] S. Johnston,[10] M. Keith,[10] A. G. Lyne,[2] P. F. Michelson,[11] P. M. Saz Parkinson,[12] S. M. Ransom,[13] P. S. Ray,[14] B. W. Stappers[2] and K. S. Wood[14]

[1]*Max-Planck-Institut für Radioastronomie, Auf dem Hügel 69, D-53121 Bonn, Germany*
[2]*Jodrell Bank Centre for Astrophysics, School of Physics and Astronomy, The University of Manchester, M13 9PL*
[3]*Columbia Astrophysics Laboratory, Columbia University, New York, NY 10027, USA*
[4]*Arecibo Observatory, HC3 Box 53995, Arecibo, PR 00612, USA*
[5]*NASA Goddard Space Flight Center, Greenbelt, MD 20771, USA*
[6]*Center for Research and Exploration in Space Science and Technology (CRESST) and NASA Goddard Space Flight Center, Greenbelt, MD 20771, USA*
[7]*Department of Physics and Center for Space Sciences and Technology, University of Maryland Baltimore County, Baltimore, MD 21250, USA*
[8]*Laboratoire de Physique et Chimie de l'Environnement, LPCE UMR 6115 CNRS, F-45071 Orléans Cedex 02, France*
[9]*Station de radioastronomie de Nançay, Observatoire de Paris, CNRS/INSU, F-18330 Nançay, France*
[10]*CSIRO Astronomy and Space Science, Australia Telescope National Facility, Epping NSW 1710, Australia*
[11]*W. W. Hansen Experimental Physics Laboratory, Kavli Institute for Particle Astrophysics and Cosmology, Department of Physics and SLAC National Accelerator Laboratory, Stanford University, Stanford, CA 94305, USA*
[12]*Santa Cruz Institute for Particle Physics, Department of Physics and Department of Astronomy and Astrophysics, University of California at Santa Cruz, Santa Cruz, CA 95064, USA*
[13]*National Radio Astronomy Observatory (NRAO), Charlottesville, VA 22903, USA*
[14]*Space Science Division, Naval Research Laboratory, Washington, DC 20375-5352, USA*

Accepted 2012 November 19. Received 2012 November 12; in original form 2012 September 10

ABSTRACT

Using the 100-m Effelsberg radio telescope operating at 1.36 GHz, we have performed a targeted radio pulsar survey of 289 unassociated γ-ray sources discovered by the Large Area Telescope (LAT) aboard the *Fermi* satellite and published in the 1FGL catalogue (Abdo et al. 2010a). This survey resulted in the discovery of millisecond pulsar J1745+1017, which resides in a short-period binary system with a low-mass companion, $M_{c,\mathrm{min}} \sim 0.0137\,\mathrm{M}_{\odot}$, indicative of 'black widow' type systems. A 2-yr timing campaign has produced a refined radio ephemeris, accurate enough to allow for phase-folding of the LAT photons, resulting in the detection of a dual-peaked γ-ray light curve, proving that PSR J1745+1017 is the source responsible for the γ-ray emission seen in 1FGL J1745.5+1018 (2FGL J1745.6+1015; Nolan et al. 2012). We find the γ-ray spectrum of PSR J1745+1017 to be well modelled by an exponentially cut-off power law with cut-off energy 3.2 GeV and photon index 1.6. The observed sources are known to contain a further 10 newly discovered pulsars which were undetected in this survey. Our radio observations of these sources are discussed and in all cases limiting flux densities are calculated. The reasons behind the seemingly low yield of discoveries are also discussed.

Key words: pulsars: general – pulsars: individual: PSR J1745+1017 – gamma-rays: general.

1 INTRODUCTION

The detection of pulsed γ-ray emission from the Crab Pulsar in the early 1970s (Vasseur et al. 1970; Grindlay 1972), the first of its kind, brought new light to the study of pulsar emission physics and high-energy emission physics in general. Gamma-ray photons

⋆ E-mail: ebarr@mpifr-bonn.mpg.de (EDB); guillemo@mpifr-bonn.mpg.de (LG)

of energies greater than 100 keV are created in processes involving nuclear or other non-thermal reactions, and as such become important when exploring the Universe at its most energetic. The current model for the creation of γ-ray photons that we see from pulsars is that charged particles stripped from the surface are accelerated to relativistic energies in the pulsar's strong electric field. As these particles travel along the curved magnetic field lines, they produce γ-ray photons via synchrotron radiation, curvature radiation (e.g. Ruderman & Sutherland 1975) and inverse Compton scattering from lower energy photons (e.g. Daugherty & Harding 1986). The study of these processes gives insight into the structure and composition of the magnetospheres of pulsars.

Prior to 2008, the most successful space-based γ-ray experiment was the *Compton Gamma-ray Observatory* (*CGRO*), which was in orbit for 9 yr and carried the Energetic Gamma-ray Experiment Telescope (EGRET; Kanbach et al. 1989). EGRET was sensitive to γ-ray photons in the range 20 MeV–30 GeV, and during its lifetime brought the known number of γ-ray emitting pulsars up to at least six (Thompson 2008). However, the legacy of EGRET for the radio community was not the pulsars it detected, but rather those sources for which it could make no positive association. Targeted radio searches of these 169 γ-ray sources, unassociated with either pulsars or blazars, were performed, leading to several pulsar discoveries (e.g. Champion, McLaughlin & Lorimer 2005; Keith et al. 2008).

The Large Area Telescope (LAT; Atwood et al. 2009) aboard the *Fermi* Gamma-ray Space Telescope, represents a significant improvement upon EGRET, providing a greater energy range and sensitivity, allowing for better measurements of source characteristics and localizations. With a host of new sources discovered, including many active galactic nuclei (AGNs) and pulsars, the *Fermi*-LAT is the most successful GeV γ-ray observatory to date. As with EGRET, it is those sources for which *Fermi* cannot immediately provide an association that have piqued the interest of the pulsar searching community. A catalogue of 1451 γ-ray sources detected above 100 MeV was created from the first 11 months of LAT data. Of these sources, 630 were unassociated with known astrophysical objects (AGNs, pulsars, etc.; Abdo et al. 2010a). Multiwavelength observations of the unassociated sources were encouraged so as to determine their natures, with many radio observatories searching for radio pulsations in the *Fermi* observational error ellipses (e.g. Cognard et al. 2011; Keith et al. 2011; Ransom et al. 2011).

While *Fermi*-LAT data have already been proved to contain a wealth of pulsars, with more than 100 pulsars detected through blind periodicity searches and phase-folding of LAT photons using known pulsar ephemerides (Ray & Saz Parkinson 2011), low photon counts introduce strong selection biases in the detection of pulsars through blind searches of the LAT data. This is due to the large amount of computation required to perform wide-parameter-space searches of sparse photon data sets. For this reason, blind searches of the LAT data currently have great difficulty in detecting millisecond pulsars (MSPs) or pulsars in binary systems.

Radio pulsation searches are subject to different biases and thus are an important alternate method for identifying LAT unassociated sources as pulsars. At the time of this writing, there have been 47 radio-loud pulsars discovered through searches of these sources, of which 41 are MSPs likely to be associated with their corresponding LAT source (Ray et al. 2012). These discoveries highlight the importance of targeted radio searches of the LAT data, as these pulsars were most likely undetected in more general surveys due to shorter integration times or lack of searching for binary motion.

Of the MSPs discovered, 10 are thought to be in 'black widow' systems where the companion star has a very low mass due to ablation by the strong wind of the pulsar (Fruchter, Stinebring & Taylor 1988). Before *Fermi* only three of these systems were known to exist outside globular clusters (Fruchter et al. 1988; Stappers et al. 1996; Burgay et al. 2006), which stresses the importance of investigating this new population of pulsars uncovered by the LAT. Those MSPs discovered which are not in black widow systems may also be of great use to current and future pulsar timing arrays for gravitational wave detection (Foster & Backer 1990), which benefit from an even distribution of precisely timed pulsars across the sky.

In this paper, we present a targeted search of 289 unassociated *Fermi* sources using the 100-m Effelsberg telescope operating at 1.36 GHz. The search has resulted in the discovery of a 2.65-ms pulsar, PSR J1745+1017, in a 17.5-h binary orbit with a 0.016-$M_\odot$ companion. The positions of 10 pulsars found in other targeted searches of unassociated LAT sources are contained within the 289 sources observed. For these sources, we discuss possible reasons for our non-detections and provide flux density limits where applicable.

This paper is structured as follows. In Section 2, we discuss selection criteria for sources to be observed. In Section 3, we discuss the observational methods and data processing. In Section 4, we discuss the survey sensitivity. In Section 5, we discuss simulations of the survey. In Section 6, we discuss the results of the survey. In Section 7, we discuss the source selection and detection rate. In Section 8, we present our conclusions.

2 *FERMI* CATALOGUE SOURCE SELECTION

All the sources searched for this paper were selected either from the *Fermi*-LAT First Source catalogue (1FGL; Abdo et al. 2010a) or from an unpublished update to the 1FGL which covered the first 18 months of *Fermi* observations.

The 1FGL contains 630 sources unassociated with any known astrophysical object, in the 100 MeV to 100 GeV energy range. The catalogue includes source localizations defined in terms of an elliptical fit to the 95 per cent confidence level, power-law spectral fits, monthly light curves and flux measurements in five energy bands for each source. A full description of the 1FGL can be found in Abdo et al. (2010a). To narrow down the number of potentially observable sources, those below -20° declination, and those for which a known association existed were ignored. For all sources, the pointing position was chosen to coincide with the centre of the error ellipse. As better source localizations became available, pointing positions were altered such that they coincided with the centre of the updated error ellipse.

The remaining sources were ranked using an application of the Gaussian-mixture model as outlined in Lee et al. (2012). The best pulsar candidates exhibit significantly curved emission spectra and little γ-ray flux variability over time, in contrast with e.g. blazars and other AGNs (see e.g. fig. 17 of Nolan et al. 2012).

The top 250 ranked candidates from the 1FGL catalogue were selected to be observed. A further 39 highly ranked sources from the 18-month update to the 1FGL were also selected to be observed, giving a total of 289 target sources.

3 OBSERVATIONAL METHOD AND DATA PROCESSING

All search data presented in this paper were taken with the 100-m Effelsberg radio telescope at a centre frequency of 1.36 GHz between 2009 November and 2010 July, using the central horn of the new Effelsberg multibeam receiver with 300-MHz bandwidth.

The 289 sources selected for this survey were observed in three different observing campaigns. Initially all sources were observed with between 10- and 16-minute integrations. These integrations allowed for a preliminary shallow sweep of all sources such that the brightest pulsars, those likely to have been of the greatest use for timing applications, could be found. The second observing campaign was comprised of 32-minute integrations on 78 sources, with special focus given to covering as many of the highest ranked sources as time allowed. Finally, in the third campaign, 70 highly ranked sources were observed with between 60- and 76-minute integrations, with 32 of these sources observed multiple times. Observing in this manner reduced the effects of scintillation and of man-made radio-frequency interference (RFI), as most sources were observed multiple times with different integration times at different observing epochs.

Data were recorded over 512 filterbank channels of width 585.3 kHz with a sampling rate of 53 μs.[1] Initially all data were sampled at 32 bits by the digitizers before being brought down to 8 bits and written to high-capacity magnetic tape for transportation and storage.

To meet the processing demands imposed by the 5.5 TB of data created in the survey, a 22-node 168-core computing cluster situated in the MPIfR was used for all data analysis. The PRESTO software package (Ransom 2001) was used for data processing.

In the first stage of the processing pipeline, data underwent RFI treatment in which a time- and frequency-dependent mask was created to be applied at a later stage. As the 1FGL catalogue contains no distance information, each beam was de-dispersed at 2760 trial dispersion measures (DMs) in the range 0–997 pc cm^{-3} to mitigate against the frequency-dependent delay in the pulsar signal due to dispersion by free electrons along the line of sight. Our choice of such a fine sampling in dispersion space allows for the retention of the data's maximum possible time resolution at all dispersion measures. The effect of this was a heightened sensitivity to millisecond and potential sub-millisecond pulsars.

All de-dispersed time series were fast-Fourier-transformed (FFT) and the resulting power spectra were de-reddened and known RFI frequencies were removed. To reconstruct power distributed through harmonics in the Fourier domain, the process of incoherent harmonic summing was used. Here the original spectra are summed with versions of themselves that have been stretched by a factor of 2 such that all second-order harmonics are added to their corresponding fundamental. This process was repeated four times such that all power distributed in even harmonics up to the 16th harmonic may be incoherently added to the fundamental (see e.g. Lorimer & Kramer 2005). The spectra from each stage of the summing process were searched for accelerated and non-accelerated signals.

At this stage the number and size of the FFTs required to achieve sensitivity to fast binaries becomes computationally too expensive for the longest pointings. To deal with this, the processing of the data was split into two stages. Initially all data were analysed at full length with a moderate acceleration search in the Fourier domain. This analysis is very sensitive to isolated and mildly accelerated pulsars in the data. The second processing stage involves splitting the data into 10-minute blocks and re-analysing with a much more intensive acceleration search. Although this stage uses shorter integrations, it is more sensitive to highly accelerated binary systems in the data. The details of the acceleration search can be found in Section 4.

Upon completion of the processing, all candidate signals underwent a sifting routine that removes any signals which are likely to be RFI. Finally, for the top 50 candidates a set of diagnostic plots were created for visual inspection (e.g. Eatough et al. 2010). In cases where there were more than 50 candidates with greater than 8σ significance, the pointing was considered to be contaminated by RFI and was flagged for re-observation.

4 SENSITIVITY

To estimate the sensitivity of our survey setup, we used the radiometer equation (see e.g. Lorimer & Kramer 2005),

$$S_{\rm min} = \beta \frac{S/N_{\rm min} T_{\rm sys}}{G\sqrt{n_p t_{\rm obs} \delta f}} \left(\frac{P_{\rm cycle}}{1 - P_{\rm cycle}} \right)^{1/2}, \quad (1)$$

where the constant factor β denotes signal degradation due to digitization, which for 8-bit digitization is ∼1 per cent, giving $\beta = 1.01$ (Kouwenhoven & Voûte 2001). $T_{\rm sys}$ is the system temperature of the receiver. From flux density calibration measurements we found $T_{\rm sys} = 25$ K. G is the antenna gain (1.5 K Jy^{-1} at 1.36 GHz), $P_{\rm cycle}$ is the pulse duty cycle, $t_{\rm obs}$ is the length of the observation, δf is the effective bandwidth of the receiver (240 MHz) and n_p is the number of polarizations summed, which for this survey is always 2. The factor $S/N_{\rm min}$ is the minimum signal-to-noise ratio with which we can make a detection. Based on false alarm statistics, we chose $S/N_{\rm min} = 8$.

Fig. 1 shows the minimum detectable flux density as a function of pulsar period for four dispersion measures: 0, 100, 500 and 1000 pc cm^{-3}. Assuming a pulsar of typical duty cycle 5 per cent,

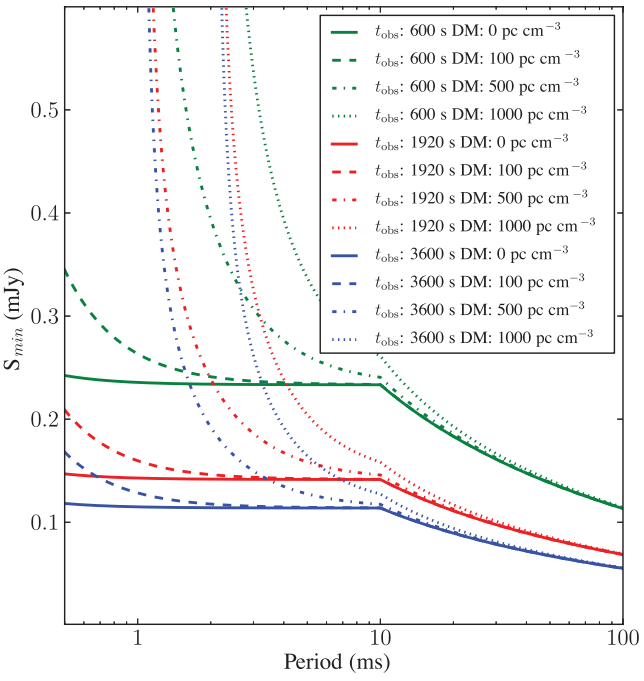

Figure 1. Theoretical minimum detectable flux densities ($S_{\rm min}$) versus spin period for three integration regimes. A minimum detectable signal-to-noise ratio of 8 was imposed. The break point at period 10 ms occurs due to the assumption that the pulse duty-cycle scales as period$^{-0.5}$ with a maximum value of 1/3 (Kramer et al. 1998).

[1] An in-depth review of the observational setup for pulsar searches with the Effelsberg telescope will be published in the initial paper of the High Time Resolution Universe North pulsar survey (Barr et al., in preparation).

we achieve a minimum detectable flux density of 0.02 mJy for a 76-minute pointing and 0.06 mJy for a 10-minute pointing.

In a binary system, due to the Doppler effect, the apparent spin frequency of the pulsar drifts with time, spreading the pulsar's power in the Fourier domain. To reconstruct Fourier power smeared across multiple bins, we employed the PRESTO *accelsearch* routine which uses the 'correlation technique' of template matching in the Fourier domain as outlined in Ransom, Eikenberry & Middleditch (2002). The relationship between the largest range of Fourier bins over which to search for drifted signals, $Z_{\rm max}$, and the acceleration to which the search is sensitive, a_0, can be described by

$$a_0 = \frac{Z_{\rm max} P c}{t_{\rm obs}^2}, \quad (2)$$

where P is the spin period of the pulsar being searched for, $t_{\rm obs}$ is the integration time and c is the speed of light in a vacuum.

By assuming a 1-ms period pulsar in a binary system, we may determine the sensitivity of the search at the extreme limit of the pulsar population. For the first processing pass, where the data were analysed in full length, we used $Z_{\rm max} = 50$ to achieve sensitivity to accelerations of up to $|a_0| \sim 42$ and 1 m s^{-2} for 10- and 76-minute integrations, respectively. For the second processing pass, where data were analysed in 10-minute blocks, we used $Z_{\rm max} = 600$ to achieve sensitivity to accelerations of up to $|a_0| \sim 500$ m s^{-2}. For all systems which fall inside the acceleration limits for their integration lengths, the minimum detectable flux density may be calculated via equation (1).

5 SIMULATIONS

As with any survey that contains many pointings, we may assume that the chance detection probability for pulsars unassociated with the LAT sources targeted is non-negligible. In order to determine this probability, simulations of the normal pulsar and MSP populations were made based on the model presented in Lorimer et al. (2006) using the PSRPOP[2] software. As the population distributions for MSPs and normal pulsars differ, separate simulations were performed for pulsars with rotational periods above and below 40 ms.

To simulate the normal pulsar distribution, input model parameters were chosen as follows.

(i) An empirical period distribution taken from the probability density function of the known population.

(ii) A log-normal luminosity distribution, with mean and variance in log space of −1.1 and 0.9, respectively (Faucher-Giguère & Kaspi 2006).

(iii) A Gaussian distribution of spectral indices, with mean of −1.6 and variance of 0.5.

(iv) An exponential distribution for the height above the Galactic plane, with a scale height of 0.33 kpc (Lorimer et al. 2006).

(v) A radial distribution as described in Lorimer et al. (2006).

(vi) The NE2001 Galactic free electron density model (Cordes & Lazio 2002).

To simulate the MSP population, the same model parameters were used with the Galactic scale height increased to 0.5 kpc to better match the known MSP distribution (Lorimer et al. 2006).

The number of pulsars simulated was such that the cumulative number of pulsars discovered in simulated versions of the Parkes Multibeam Pulsar Survey (Manchester et al. 2001), the Swinburne Intermediate-Latitude Pulsar Survey (Edwards et al. 2001) and its extension (Jacoby et al. 2009), and the Parkes High-Latitude Survey (Burgay et al. 2006), matched the real discovery numbers.

Each observation of the 289 sources in the survey was then compared against the simulated pulsar distribution to determine if a chance detection could have been made. The Galactic pulsar population was simulated 1000 times and comparisons repeated with each simulation. We find a mean detection rate of 0.4 normal pulsars and 0.04 MSPs in the 289 pointings. While not ruling out the possibility of a chance MSP detection, these figures suggest that any MSP found in this survey will be associated with the LAT source targeted at 96 per cent confidence.

6 RESULTS

6.1 PSR J1745+1017

6.1.1 Radio analysis

The main result of this work is the discovery of the radio pulsar PSR J1745+1017 in LAT source 1FGL J1745.5+1018 (2FGL J1745.6+1015). Initially discovered as a mildly accelerated candidate in a 10-minute data segment, PSR J1745+1017 has a period of 2.65 ms and a period derivative of 2.72×10^{-21}, making it the first MSP discovered with the Effelsberg telescope.

Upon discovery, PSR J1745+1017 was the subject of an intensive timing campaign involving the Effelsberg, Lovell and Nançay radio telescopes. Pulse times of arrival (TOAs) were analysed with the TEMPO2 software package (Hobbs, Edwards & Manchester 2006) to create a phase-connected timing solution for the first 2 yr of radio observations. The pulsar ephemeris and a selection of derived properties are displayed in Table 1.

From period and period derivative measurements, we infer a characteristic age of 16.9 Gyr. Combined with the rapid spin period of PSR J1745+1017, this implies that the pulsar has undergone an extensive period of accretion-induced spin-up due to mass transfer from a companion star. This hypothesis is supported by the timing solution, which shows PSR J1745+1017 to be in a low-eccentricity binary system with an orbital period of 17.5 h and a low-mass companion. Using the definition for the binary mass function,

$$f(m_1, m_2) = \frac{4\pi^2}{G}\frac{(a \sin i)^3}{P_b^2} = \frac{(m_2 \sin i)^3}{(m_1 + m_2)^2}, \quad (3)$$

where m_1 and m_2 are the masses of the pulsar and companion, respectively; G is Newton's gravitational constant; $a \sin i$ is the projected semi-major axis of the system, where i is the inclination angle of the binary (defined such that $i = 90^\circ$ is edge on) and P_b is the orbital period, we obtain $f(m_1, m_2) = 1.4 \times 10^{-6}$ M$_\odot$. Assuming an average pulsar mass of 1.35 M$_\odot$, this gives minimum and median companion masses of 0.014 and 0.016 M$_\odot$, respectively.

This small range of low companion masses strongly suggests that PSR J1745+1017 is a black widow system with a white dwarf companion that has been heavily ablated by the strong particle wind from the pulsar. Unlike black widow systems such as PSR B1957+21 (Fruchter et al. 1988) and PSR J2051−0827 (Stappers et al. 1996), PSR J1745+1017 exhibits neither eclipsing behaviour nor DM variations across orbital phase, implying a low-inclination angle. If the inclination is low, then the companion mass is likely to be larger than the presented value. As noted by Lorimer & Kramer (2005), the probability of observing a binary system with an inclination less than i_0 for a random distribution of orbital inclinations is $p(i) = 1 - \cos(i_0)$. This relation suggests that the inclination angle

[2] http://psrpop.phys.wvu.edu/index.php

Table 1. PSR J1745+1017 ephemeris created from TOAs taken with the Nançay, Effelsberg and Lovell telescopes over the course of 22 months. Numbers in parentheses represent twice the formal 1σ uncertainties in the trailing digit as determined by TEMPO2. The dispersion-measure-derived distance was estimated using the NE2001 Galactic electron density model (Cordes & Lazio 2002). Due to intrinsic uncertainties in this model, the estimation is likely to have an uncertainty of ∼20 per cent. The mass function calculation assumes an average mass of 1.35 $M_\odot$ for the pulsar. The characteristic age, spin-down luminosity and surface magnetic field strengths were calculated using the Shklovskii-corrected period derivative. The position, frequency and DM are all measured with respect to the given reference epoch. These parameters were determined with TEMPO2, which uses the International Celestial Reference System and Barycentric Coordinate Time. Refer to Hobbs et al. (2006) for information on modifying this timing model for observing systems that use TEMPO format parameters.

PSR J1745+1017 ephemeris	
Fitted timing parameters	
Right ascension (RA J2000) (hh:mm:ss)	17:45:33.8371(7)
Declination (Dec. J2000) (°:′:″)	+10:17:52.523(2)
Proper motion:	
in R.A. (μ_α cos(Dec.)) (mas yr^{-1})	6(1)
in Decl. (μ_δ) (mas yr^{-1})	−5(1)
Period (s)	0.002 652 129 671 08(3)
Period derivative ($\times 10^{-21}$)	2.73(1)
Dispersion measure (pc cm^{-3})	23.970(2)
Orbital period (d)	0.730 241 444(1)
Projected semimajor axis (lt-s)	0.088 172(1)
Epoch of ascending node (MJD)	552 09.968 794(2)
κ ($\equiv e\cos\omega$) ($\times 10^{-5}$)	0(2)
η ($\equiv e\sin\omega$) ($\times 10^{-5}$)	0(2)
Fixed parameters	
Reference epoch (MJD)	554 00
Clock correction procedure	TT(TAI)
Time system	TCB
Solar system ephemeris model	DE414
Binary model	ELL1 (Lange et al. 2001)
Derived parameters	
Frequency (Hz)	377.055 470 138 13(5)
Frequency derivative (Hz s^{-1} $\times 10^{-16}$)	−3.88(2)
Orbital eccentricity ($\times 10^{-5}$)	0(2)
Epoch of periastron passage (MJD)	552 10.3(4)
Galactic longitude (J2000) (deg)	34.°869 3081(3)
Galactic latitude (J2000) (deg)	19.°253 6887(5)
Mass function ($M_\odot$)	1.38(1)$\times 10^{-6}$
Minimum companion mass ($M_\odot$)	0.0137
Median companion mass ($M_\odot$)	0.0158
Dispersion-measure-derived distance (kpc)	1.3(2)
Shklovskii-corrected period derivative ($\times 10^{-21}$)	2.22(5)
Characteristic age (Gyr)	18.9
Spin-down luminosity ($\times 10^{33}$ erg s^{-1})	4.7
Surface magnetic field ($\times 10^7$ G)	7.7
rms residual (μs)	5.05
Further parameters	
Median flux density at 1.36 GHz (mJy)	0.3
Maximum flux density at 1.36 GHz (mJy)	4.4
Span of timing data (MJD)	55 225–560 26
Number of TOAs	156

is greater than 26° at 90 per cent confidence. We therefore place an upper limit of 0.032 $M_\odot$ on the mass of the companion to the same confidence level.

From proper motion measurements of PSR J1745+1017, we find a transverse velocity of ∼48 ± 9 km s^{-1}. The small dispersion-measure-inferred distance to this pulsar, $d \sim 1.3$ kpc, suggests that the Shklovskii effect (Shklovskii 1970) contribution to the measured period derivative will be non-negligible. For a pulsar with transverse velocity v_t, the Shklovskii effect acts to increase the intrinsic period derivative of the pulsar by a factor Pv_t/cd (see Camilo, Thorsett & Kulkarni 1994), where c is the speed of light in a vacuum. We find a contribution to the period derivative of $5 \pm 2 \times 10^{-23}$ or about 18 per cent of the measured value.

Assuming a moment of inertia of 10^{45} g cm^2 and using the Shklovskii-corrected period derivative, we derive the spin-down luminosity of PSR J1745+1017 to be $\dot{E} = 4\pi^2 I \dot{P}/P^3 = 4.7 \times 10^{33}$ ergs s^{-1}, a value which makes this pulsar a good candidate for pulsed γ-ray emission (Abdo et al. 2010a).

6.1.2 *Gamma-ray analysis*

In order to characterize the γ-ray emission of PSR J1745+1017, we selected *Fermi*-LAT data recorded between 2008 August 4 and 2012 March 7, with reconstructed energies larger than 0.1 GeV, directions within a circular region of interest (ROI) of 15° radius around the pulsar's position, and zenith angles smaller than 100°. We further restricted the data set to 'Source' class events of the P7_V6 instrument response functions (IRFs), and rejected times when the rocking angle of the LAT exceeded 52° or when the Earth's limb infringed upon the ROI. The selected γ-ray events were finally phase-folded using the ephemeris given in Table 1 and the *Fermi* plug-in distributed with TEMPO2 (Ray et al. 2011).

Initial pulsation searches using standard data selection cuts yielded marginal detections only. For instance, selecting photons found within 1° of the pulsar and with energies larger than 0.1 GeV, we found an *H*-test parameter (de Jager & Büsching 2010) of 15.6, which translates to a significance of $\sim 3.1\sigma$. Nonetheless, pulsation searches can be made more sensitive by weighting the photons by the probability that they originate from the pulsar. These probabilities can be computed through a spectral analysis of the pulsar and the neighbouring sources (Kerr 2011; Guillemot et al. 2012).

The γ-ray spectrum of PSR J1745+1017 was measured by fitting sources in the ROI using a binned likelihood method, with the *pyLikelihood* module included in the *Fermi* Science Tools.[3] The source model used for the analysis included the spectral parameters of the 78 sources of the *Fermi*-LAT Second Source Catalogue (2FGL; Nolan et al. 2012) found within 20° of the pulsar. The spectrum of PSR J1745+1017 was represented by an exponentially cut-off power-law of the form $\mathrm{d}N/\mathrm{d}E = N_0(E/1\,\mathrm{GeV})^{-\Gamma}\exp(-E/E_c)$, where N_0 is a normalization factor, Γ is the photon index and E_c is the cut-off energy. The extragalactic diffuse emission and the residual instrument background were modelled using the *iso_p7v6source* template, and the Galactic diffuse emission was modelled using the *gal_2yearp7v6_v0* map cube. The spectral parameters of the sources within 5° of the pulsar as well as the normalizations of the diffuse models were re-fitted, while the parameters of other sources were fixed at the 2FGL catalogue values. We found no evidence of significant emission from the pulsar in the phase range [0.6; 1]. In order to increase the signal-to-noise ratio of the pulsar, we thus restricted the

[3] http://fermi.gsfc.nasa.gov/ssc/data/analysis/scitools/overview.html

Table 2. Measured γ-ray light curve and spectral parameters for PSR J1745+1017. First quoted uncertainties are statistical, and the second are systematic. Details on the determination of the systematic uncertainties are given in Section 6.1.2.

Parameter	Value
First peak position, Φ_1	0.14 ± 0.04
First peak full width at half-maximum, FWHM_1	0.20 ± 0.16
Second peak position, Φ_2	0.39 ± 0.03
Second peak full width at half-maximum, FWHM_2	0.10 ± 0.10
Radio to γ-ray lag, δ	0.14 ± 0.04
γ-ray peak separation, Δ	0.26 ± 0.06
Photon index, Γ	$1.6 \pm 0.2^{+0.1}_{-0.1}$
Cut-off energy, E_c (GeV)	$3.2 \pm 1.2^{+0.2}_{-0.1}$
Photon flux (>0.1 GeV), F_{100} (10^{-8} cm^{-2} s^{-1})	$1.1 \pm 0.3^{+0.1}_{-0.1}$
Energy flux (>0.1 GeV), G_{100} (10^{-12} erg cm^{-2} s^{-1})	$9.3 \pm 1.2^{+0.3}_{-0.6}$
Luminosity, L_γ / f_Ω (10^{33} erg s^{-1})	$1.8 \pm 0.6^{+0.6}_{-0.6}$
Efficiency, η / f_Ω	$0.3 \pm 0.1^{+0.1}_{-0.1}$

data set to photons with reconstructed pulse phases between 0 and 0.6 (the γ-ray light curve of PSR J1745+1017, presented below, is indeed compatible with showing emission only in this phase range). The best-fitting spectral parameters of PSR J1745+1017 are listed in Table 2, along with the integrated photon and energy fluxes above 0.1 GeV derived from these results. Systematic uncertainties were calculated by running the same analysis as described above, but using bracketing IRFs for which the effective area has been perturbed by ±10 per cent at 0.1 GeV, ±5 per cent near 0.5 GeV and ±10 per cent at 10 GeV, with linear interpolations in log space between.

Using the best-fitting spectral model for the ROI obtained from the analysis described above, we could calculate probabilities that the photons in the ROI originate from PSR J1745+1017. Selecting events found within 5° and with calculated probabilities larger than 0.01, we obtained a weighted *H*-test parameter (see Kerr 2011) of 58.0, corresponding to a pulsation significance of 6.5σ. Fig. 2 shows probability-weighted light curves for PSR J1745+1017 in different energy bands. The background levels shown in Fig. 2 were calculated by summing the probabilities that selected γ-ray events do not originate from the pulsar, as described in Guillemot et al. (2012). Statistical error bars were obtained by calculating $\sqrt{\sum_i w_i^2}$, where w_i represents the photon probability and i runs over photons falling in the same phase bin (Pletsch et al. 2012). As can be seen from Fig. 2, the γ-ray profile of PSR J1745+1017 shows evidence for two distinct peaks, at phases ∼0.14 and ∼0.39. Fits of the two γ-ray peaks with Lorentzian pulse shapes above 0.3 GeV yielded the peak positions Φ_i and the full widths at half maxima FWHM_i listed in Table 2. We also attempted to fit the light curve with one asymmetric Lorentzian pulse shape, and found that the model with two peaks is slightly preferred, at the $\sim 1\sigma$ level. The radio to γ-ray lag $\delta = \Phi_1 - \Phi_r$ (where $\Phi_r = 0$ is the phase of the maximum of the radio profile shown in Fig. 2) and the γ-ray peaks separation $\Delta = \Phi_2 - \Phi_1$ are found to be $\delta = 0.14 \pm 0.04$ and $\Delta = 0.26 \pm 0.06$, respectively (see Table 2). The uncertainty on the radio to γ-ray lag due to the error on the measurement of the DM parameter is estimated to be $\Delta(\delta) = \Delta(\mathrm{DM})/(Kf^2)$, where $K = 2.410 \times 10^{-4}$ MHz^{-2} cm^{-3} pc s^{-1} is the dispersion constant. We find $\Delta(\delta) \sim 10^{-3} \times P$, which is very small compared to the statistical error bar. Such values of δ and Δ are relatively common amongst other known γ-ray pulsars (see fig. 4 of Abdo et al. 2010b), and match the predictions of theoretical models that place the high-

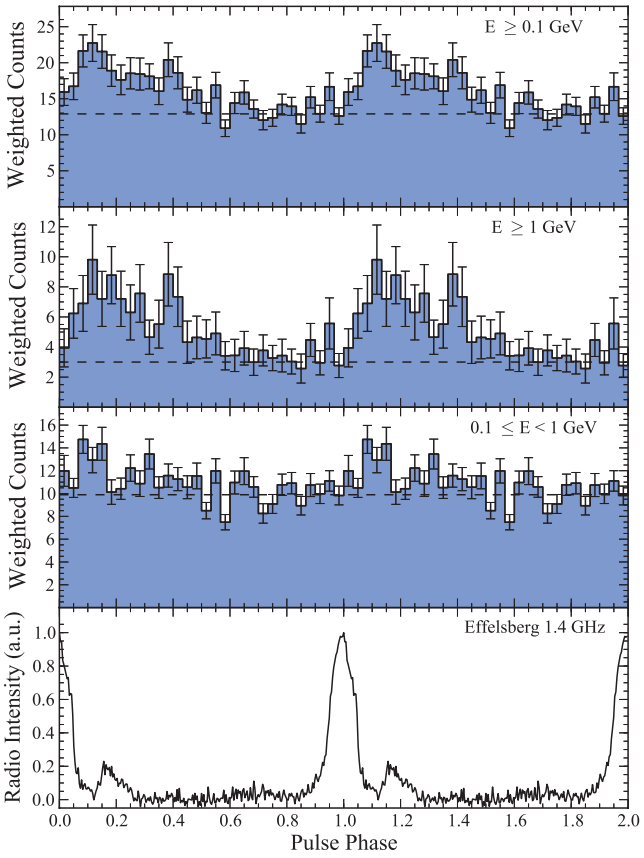

Figure 2. Multiwavelength light curves of PSR J1745+1017. The bottom panel shows the 1.4 GHz radio profile recorded with the Effelsberg radio telescope. The upper panels show probability-weighted γ-ray light curves in different energy ranges, with 30 bins per rotation. The horizontal dashed lines show the estimated γ-ray background levels. Two rotations are shown for clarity.

energy emission from pulsars at high altitudes in the magnetosphere (Romani & Yadigaroglu 1995).

The ephemeris used for phase-folding the γ-ray data considered in this analysis is based on radio timing taken after 2010 January 30 (MJD 552 26). In an attempt to determine whether the ephemeris describes the rotational behaviour of the pulsar over the entire *Fermi*-LAT data set accurately, we analysed the evolution of the weighted *H*-test parameter as a function of time. The results of this analysis are shown in Fig. 3. First of all, because the *H*-test depends linearly on the number of photons for a given pulsed signal fraction, the linear increase of the *H*-test parameter as a function of the data set length provides further evidence that the pulsed γ-ray signal from PSR J1745+1017 is real. Moreover, the increase of the *H*-test parameter when going forward or backward in time is monotonic outside the formal ephemeris validity interval, which indicates that the ephemeris given in Table 1 provides a good description of the pulsar's rotational behaviour across the entire LAT data set.

From the energy flux G_{100} measured from the spectral analysis, we calculated the γ-ray luminosity above 0.1 GeV using $L_\gamma = 4\pi f_\Omega G_{100} d^2$, where f_Ω is a geometrical correction factor depending on the beaming angle of the pulsar and the viewing geometry (Watters et al. 2009). Using the distance derived from the NE2001 model of $d = 1.3 \pm 0.2$ kpc, we get the γ-ray luminosity $L_\gamma / f_\Omega \sim 1.8 \times 10^{33}$ erg s^{-1} and the γ-ray efficiency, $\eta / f_\Omega = L_\gamma / \dot{E} \sim 0.3$. This value for the efficiency lies well within

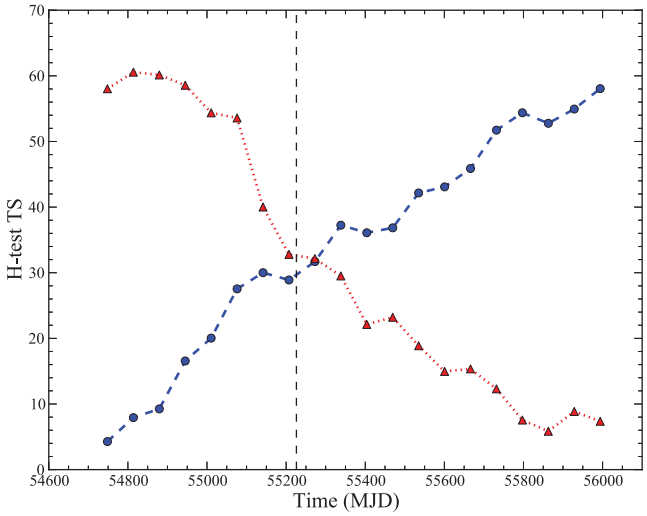

Figure 3. Evolution of the weighted *H*-test test statistic (TS) as a function of time. The blue, dashed line indicates the weighted *H*-test parameter with increasing time, using data taken from 2008 August 8. The red, dotted line indicates the weighted *H*-test parameter when going backwards in time, using data taken before 2012 March 7. The vertical, dashed line indicates the formal start of the ephemeris validity interval.

the distribution of γ-ray efficiencies seen for other LAT-detected MSPs (Abdo et al. 2010b).

From the measurement of the γ-ray energy flux and the proper motion of the pulsar, we can put an upper limit on the distance derived from the inequality $L_\gamma < \dot{E}$ (see equation 2 of Guillemot et al. 2012). Assuming $I = 10^{45}$ g cm^2 and $f_\Omega = 1$ (a typical value for other γ-ray MSPs; see e.g. Venter, Harding & Guillemot 2009), we get $d \leq 1.9$ kpc.

6.2 Radio pulsar non-detections

During the course of the observations, other observatories discovered six radio-emitting pulsars associated with the sources observed in this survey. These pulsars were not detected in this survey due to a combination of reasons, such as limited flux density, local RFI conditions and source position redefinitions. Further information on all sources observed in this work may be found in the corresponding online material, with the 15 highest ranked sources presented in Table A1.

6.2.1 PSR J2030+3641

PSR J2030+3641 (Camilo et al. 2012), initially undetected in our data processing, exhibits a rotational frequency which is similar to the 10th sub-harmonic of the 50-Hz local mains frequency. Unfortunately signals which are similar in frequency to harmonics of the mains are often lost in noise or excised from the data in the process of Fourier RFI excision, wherein known RFI signals are removed from the power spectrum of the observation prior to pulse detection. It should be noted that this pulsar was discovered using the Robert C. Byrd Green Bank Telescope in the US, where the mains frequency is 60 Hz.

Reprocessing of these data with the published ephemeris yielded a detection of the pulsar at signal-to-noise ratio 6.4, a value which lies below the detection threshold of this survey. Using equation (1), we found a corresponding estimated flux density of 0.08 mJy. This value is half that of the published flux density at 1.5 GHz, a discrepancy which may be attributed to the extra noise induced by the oscillations of the mains electricity at the folding period. It should be noted, that the derived position of J2030+3641 is coincident with the position observed in this survey.

Table 3. Limiting flux densities ($S_{\rm min}$) for LAT detected pulsars coincident with sources observed in this work. All pulsars are assumed to have a radio pulse with a 10 per cent duty cycle and scattering effects are ignored. It should be noted that the upper radio flux limits presented here are higher than those published in Pletsch et al. (2012), due to the use of an increased detection threshold of signal-to-noise 8.

PSR	Pointing offset (°)	$S_{\rm min}$ (mJy)	Reference
J0734−1559	0.05	0.1	Saz Parkinson (2011)
J1803−2149	0.05	0.1	Pletsch et al. (2012)
J2030+4415	0.02	0.08	Pletsch et al. (2012)
J2139+4716	0.04	0.09	Pletsch et al. (2012)

6.2.2 PSRs J1646−2142, J1816+4510 and J1858−2218

PSRs J1646−2142, J1858−2218 (Ray et al. 2012) and J1816+4510 (Kaplan et al. 2012) were all discovered at LAT positions that were significantly different from the position determined in the 1FGL catalogue. Because of this, the discovery position of these pulsars is a half-beamwidth or more away from the position observed in this work, and so no detection is expected.

6.2.3 PSRs J0307+7443 and J1828+0625

PSRs J0307+7443 and J1828+0625 (Ray et al. 2012) were both discovered at positions coincident with sources observed in this survey. Both pulsars were detected at low radio frequency and appear to be weak radio emitters. Assuming similar profile characteristics at both 1.36 GHz and at the discovery frequency, we found upper limits of 0.1 and 0.2 mJy on the radio flux densities at 1.36 GHz for PSRs J0307+7443 and J1828+0625, respectively.

6.3 Gamma-ray pulsar non-detections

Through blind searches of *Fermi*-LAT photons, a further four pulsars associated with the sources observed have since been discovered (Saz Parkinson 2011; Pletsch et al. 2012). No radio detection has so far been made for these pulsars, therefore in Table 3 we present our upper limits on their radio flux densities at 1.36 GHz.

A simple model for the telescope beam was used to adjust limiting flux densities for position offsets between the pointing and true position of the source. Limiting flux densities were divided by a factor q, given by $q = \mathrm{e}^{-(\theta/\phi)^2/1.5}$, where θ is the pointing offset and ϕ is the beam half-width at half-maximum, to return the true limiting flux density at 1.36 GHz ($S_{\rm min}$).

7 DISCUSSION

Considering the success that other surveys of unassociated *Fermi*-LAT sources have had (Cognard et al. 2011; Keith et al. 2011; Ransom et al. 2011; Camilo et al. 2012), we must consider the reasons behind our relatively small yield of discoveries.

Sources observed in this work were selected based on information provided in the 1FGL catalogue. However, in the recently published 2FGL catalogue, many of these sources are no longer listed. A detailed description of the possible causes for this can be found in

section 4.2 of Nolan et al. (2012). Using the 2FGL catalogue to examine the 289 sources selected for observation, we find:

(i) 106 sources that are no longer listed;
(ii) 46 sources that have moved by more than half the FWHM of the telescope beam;
(iii) 22 sources marked as potentially spurious.

Selecting against these sources and choosing only sources for which the entire updated 95 per cent confidence region was contained within the FWHM of the telescope beam, we are left with 72 sources for which observations adequately cover the LAT source targeted.

This would suggest that the detection rate for the survey is ∼1.4 per cent. However, as noted by Camilo et al. (2012), a large number of pulsar surveys at radio wavelengths have focused on observing the Galactic plane at low latitudes, introducing a strong bias against the discovery of new radio-emitting pulsars in this volume. Selecting only those 58 sources that lie in the region $|b| > 3^{\circ}.5$, we find the detection rate to be 1.7 per cent.

We note that the strategy employed by other surveys of LAT unassociated sources has generally been to select a small number of sources and observe with long integration times, often at lower frequencies (e.g. Ransom et al. 2011). By contrast, we have selected a large number of sources and observed at various integration lengths at higher frequency. Although this strategy has lacked the discoveries that other searches have made, it has provided the most complete picture yet of the LAT sky at high radio frequencies.

The results of our survey suggest that future surveys of unassociated LAT sources would benefit from lower observing frequencies, as wider beam-widths will increase the LAT error ellipse coverage, which, when combined with the decrease in LAT error ellipse size due to increasing observation depth, will significantly reduce the problems associated with source redefinitions. Furthermore, we note that the majority of pulsars discovered through radio searches of the LAT data have been found at low frequencies. This suggests that this population of pulsars may have particularly steep spectral indices. Continued multifrequency study of pulsars discovered in unassociated LAT sources will deny or confirm this hypothesis.

8 CONCLUSION

We have performed repeated observations of 289 unassociated sources from the First *Fermi*-LAT catalogue of γ-ray sources, resulting in the discovery of PSR J1745+1017.

PSR J1745+1017 has a 2.65-ms spin period and orbits a very low mass companion with an orbital period of 17.5 h. The low mass of the companion suggests that PSR J1745+1017 is a black widow system; however, a two-year timing campaign has thus far found no evidence of eclipses, dispersion measure variations across orbital phase or Shapiro delay. By performing weighted-probability analysis of LAT photons in the ROI around PSR J1745+1017, we also detected γ-ray pulsations from the source. This gives a clear indication that PSR J1745+1017 is responsible for the γ-ray emission seen from 1FGL J1745.5+1018 (2FGL J1745.6+1015).

The observed sample contains three radio pulsars, newly discovered through similar searches performed by other observatories, and four γ-ray-selected, radio-quiet pulsars, found through blind searches of *Fermi*-LAT data.

No radio detection was made for the four γ-ray-selected pulsars contained in our sample. The upper limits on their radio flux densities at 1.36 GHz were calculated. These limits can be found in Table 3.

Of the three newly discovered radio pulsars coincident with LAT sources searched in this survey, only PSR J2030+3641 was detected using the known timing solution. PSRs J0307+7443 and J1828+0625 were suspected to have radio flux densities at 1.36 GHz lower than the limiting flux density of our observations.

ACKNOWLEDGMENTS

This work was carried out based on observations with the 100-m telescope of the MPIfR (Max-Planck-Institut für Radioastronomie) at Effelsberg.

The *Fermi*-LAT Collaboration acknowledges generous ongoing support from a number of agencies and institutes that have supported both the development and the operation of the *Fermi*-LAT as well as scientific data analysis. These include the National Aeronautics and Space Administration and the Department of Energy in the US, the Commissariat à l'Energie Atomique and the Centre National de la Recherche Scientifique/Institut National de Physique Nucléaire et de Physique des Particules in France, the Agenzia Spaziale Italiana and the Istituto Nazionale di Fisica Nucleare in Italy, the Ministry of Education, Culture, Sports, Science and Technology (MEXT), High Energy Accelerator Research Organization (KEK), and Japan Aerospace Exploration Agency (JAXA) in Japan, and the K. A. Wallenberg Foundation, the Swedish Research Council and the Swedish National Space Board in Sweden.

Additional support for science analysis during the operations phase is gratefully acknowledged from the Istituto Nazionale di Astrofisica in Italy and the Centre National d'Études Spatiales in France.

The Nançay Radio Observatory is operated by the Paris Observatory, associated with the French Centre National de la Recherche Scientifique (CNRS).

JPWV acknowledges support by the European Union under Marie-Curie Intra-European Fellowship 236394.

PCCF and JPWV acknowledge support by the European Research Council under ERC Starting Grant Beacon (contract no. 279702).

We would like to thank Matthew Kerr for his input regarding initial source selection. Pulsar research and observations at Jodrell Bank Observatory have been supported through Rolling Grants from the UK Science and Technology Facilities Council (STFC).

REFERENCES

Abdo A. A. et al., 2010a, ApJS, 188, 405
Abdo A. A. et al., 2010b, ApJS, 187, 460
Atwood W. B. et al., 2009, ApJ, 697, 1071
Burgay M. et al., 2006, MNRAS, 368, 283
Camilo F., Thorsett S. E., Kulkarni S. R., 1994, ApJ, 421, L15
Camilo F. et al., 2012, ApJ, 746, 39
Champion D. J., McLaughlin M. A., Lorimer D. R., 2005, MNRAS, 364, 1011
Cognard I. et al., 2011, ApJ, 732, 47
Cordes J. M., Lazio T. J. W., 2002, arXiv:astro-ph/0207156v3
Daugherty J. K., Harding A. K., 1986, ApJ, 309, 362
de Jager O. C., Büsching I., 2010, A&A, 517, L9
Eatough R. P., Molkenthin N., Kramer M., Noutsos A., Keith M. J., Stappers B. W., Lyne A. G., 2010, MNRAS, 407, 2443
Edwards R., Bailes M., van Straten W., Britton M., 2001, MNRAS, 326, 358
Faucher-Giguère C., Kaspi V. M., 2006, ApJ, 643, 332
Foster R. S., Backer D. C., 1990, ApJ, 361, 300
Fruchter A. S., Stinebring D. R., Taylor J. H., 1988, Nat, 333, 237

Grindlay J. E., 1972, ApJ, 174, L9
Guillemot L. et al., 2012, ApJ, 744, 33
Hobbs G. B., Edwards R. T., Manchester R. N., 2006, MNRAS, 369, 655
Jacoby B. A., Bailes M., Ord S. M., Edwards R. T., Kulkarni S. R., 2009, ApJ, 699, 2009
Kanbach G. et al., 1989, Space Sci. Rev., 49, 69
Kaplan D. L. et al., 2012, ApJ, 753, 174
Keith M. J., Johnston S., Kramer M., Weltevrede P., Watters K. P., Stappers B. W., 2008, MNRAS, 389, 1881
Keith M. J. et al., 2011, MNRAS, 414, 1292
Kerr M., 2011, ApJ, 732, 38
Kouwenhoven M. L. A., Voûte J. L. L., 2001, A&A, 378, 700
Kramer M., Xilouris K. M., Lorimer D. R., Doroshenko O., Jessner A., Wielebinski R., Wolszczan A., Camilo F., 1998, ApJ, 501, 270
Lange C., Camilo F., Wex N., Kramer M., Backer D., Lyne A., Doroshenko O., 2001, MNRAS, 326, 274
Lee K. J., Guillemot L., Yue Y. L., Kramer M., Champion D. J., 2012, MNRAS, 424, 2832
Lorimer D., Kramer M., 2005, Handbook of Pulsar Astronomy, Cambridge Univ. Press, Cambridge
Lorimer D. R. et al., 2006, MNRAS, 372, 777
Manchester R. et al., 2001, MNRAS, 328, 17
Nolan P. L. et al., 2012, ApJS, 199, 31
Pletsch H. J. et al., 2012, ApJ, 744, 105
Ransom S. M., 2001, PhD thesis, Harvard University
Ransom S. M., Eikenberry S. S., Middleditch J., 2002, ApJ, 124, 1788
Ransom S. M. et al., 2011, ApJ, 727, L16
Ray P. S., Saz Parkinson P. M., 2011, in Torres D. F., Rea N., eds, Astrophysics and Space Science Proceeding: High-Energy Emission from Pulsars and their Systems. Springer, Berlin, Heidelberg, p. 21
Ray P. S. et al., 2011, ApJS, 194, 17
Ray P. S., Abdo A. A., Parent D., Bhattacharya D., Bhattacharya B., Camilo F., Cognard I., Theureau G., 2012, in 2011 Fermi Symposium Proceedings, arXiv:1205.3089
Romani R. W., Yadigaroglu I.-A., 1995, ApJ, 438, 314
Ruderman M. A., Sutherland P. G., 1975, ApJ, 196, 51
Saz Parkinson P. M., 2011, arXiv:1101.3096, p. 48
Shklovskii I., 1970, SvA, 13, 562
Stappers B. W. et al., 1996, ApJ, 465, L119
Thompson D. J., 2008, Rep. Prog. Phys., 71, 116901
Vasseur J. et al., 1970, Nat, 226, 534
Venter C., Harding A. K., Guillemot L., 2009, ApJ, 707, 800
Watters K. P., Romani R. W., Weltevrede P., Johnston S., 2009, ApJ, 695, 1289

APPENDIX A: SAMPLE POINTING INFORMATION

Table A1. Sample of observed sources as ranked by the 2FGL logarithmic likelihood, 2FGL R_s, found through application of Gaussian-mixture modelling (Lee et al. 2012) to the 2FGL catalogue. R_{95} values are the major axes of the 95 per cent error ellipses for each source as found in the 1FGL and 2FGL catalogues. Limiting flux densities are calculated by the method outlined in Section 4, with a 10 per cent duty cycle imposed. Both Galactic coordinates, *l* and *b*, and equatorial coordinates, RA and Dec., show the true pointing position of each observation. A complete table of all sources observed can be found in electronic form online.

Index	1FGL name	2FGL name	*l* (°)	*b* (°)	RA (J2000)	Dec. (J2000)	Offset from 2FGL (°)	1FGL R_{95} (°)	2FGL R_{95} (°)	Observations (minutes)	Limiting flux density (mJy)	1FGL R_s	2FGL R_s
1	J1906.6+0716c	J1906.5+0720	41.13	−0.03	19:06:36	+07:16:41	0.06	0.05	0.06	32	0.10	11.9	18.2
			41.13	−0.03	19:06:36	+07:16:41	0.06			10	0.18		
			41.13	−0.03	19:06:36	+07:16:41	0.06			60	0.07		
			41.13	−0.03	19:06:36	+07:16:41	0.06			60	0.07		
2	J1819.4−1518c	J1819.3−1523	15.70	−0.05	18:19:25	−15:18:26	0.09	0.12	0.12	36	0.09	7.27	15.5
			15.70	−0.05	18:19:25	−15:18:26	0.09			26	0.11		
			15.70	−0.05	18:19:25	−15:18:26	0.09			60	0.07		
			15.70	−0.05	18:19:25	−15:18:26	0.09			10	0.18		
3	J1932.1+1914c	J1932.1+1913	54.61	0.10	19:32:10	+19:14:33	0.02	0.07	0.07	32	0.10	7.57	13.8
			54.61	0.10	19:32:10	+19:14:33	0.02			10	0.18		
4	J1846.8−0233c	J1847.2−0236	30.12	−0.14	18:46:48	−02:33:46	0.12	0.13	0.11	32	0.10	6.85	13.4
			30.12	−0.14	18:46:48	−02:33:46	0.12			10	0.18		
5	J1625.3−0019	J1625.2−0020	13.95	31.81	16:25:20	−00:19:31	0.03	0.08	0.06	32	0.10	4.36	12.2
			13.95	31.81	16:25:20	−00:19:31	0.03			60	0.07		
			13.92	31.83	16:25:13	−00:20:11	0.00			60	0.07		
6	J0224.0+6201c	J0224.0+6204	133.56	1.07	02:24:02	+62:01:00	0.06	0.07	0.06	32	0.10	11.9	12.2
			133.56	1.07	02:24:02	+62:01:01	0.06			60	0.07		
			133.55	1.09	02:24:01	+62:02:17	0.04			76	0.06		
7	J2030.9+4411	J2030.7+4417	82.30	2.84	20:30:55	+44:11:52	0.10	0.09	0.07	10	0.18	8.21	12
			82.30	2.84	20:30:55	+44:11:52	0.10			60	0.07		
			82.30	2.84	20:30:55	+44:11:52	0.10			60	0.07		
			82.30	2.84	20:30:55	+44:11:52	0.10			32	0.07		
8	J1857.9+0352c	J1857.8+0355c	37.13	0.31	18:57:60	+03:52:43	0.05	0.07	0.16	32	0.10	12.7	11.9
			37.14	0.29	18:58:06	+03:52:43	0.08			10	0.18		
9	J2030.0+3641	J2030.0+3640	76.12	−1.44	20:30:00	+36:41:02	0.01	0.06	0.04	10	0.18	9.82	11.8
10	J0308.6+7442	J0308.3+7442	131.75	14.24	03:08:37	+74:42:42	0.07	0.10	0.06	32	0.10	3.57	11.7
			131.71	14.25	03:08:16	+74:44:14	0.03			60	0.07		
11	J0608.3+2038c	J0608.3+2037	189.76	0.29	06:08:20	+20:38:07	0.00	0.09	0.11	32	0.10	4.4	9.89
			189.76	0.28	06:08:20	+20:38:07	0.00			10	0.18		
			189.76	0.27	06:08:16	+20:37:59	0.02			60	0.07		
			189.76	0.27	06:08:16	+20:37:59	0.02			60	0.07		
12	J2032.8+3928	J2033.6+3927	78.69	−0.24	20:32:48	+39:28:12	0.21	0.25	0.12	32	0.10	1.65	9.68
13	J0426.5+5437	J0426.7+5434	150.84	3.87	04:26:35	+54:37:51	0.06	0.14	0.11	32	0.10	2.99	9.38
			150.84	3.87	04:26:35	+54:37:51	0.06			10	0.18		
			150.84	3.87	04:26:35	+54:37:52	0.07			60	0.07		
			150.82	3.85	04:26:24	+54:38:17	0.10			32	0.10		
			150.82	3.85	04:26:24	+54:38:17	0.10			60	0.07		

Table A1 – *continued*

Index	1FGL name	2FGL name	l (°)	b (°)	RA (J2000)	Dec. (J2000)	Offset from 2FGL (°)	1FGL R_{95} (°)	2FGL R_{95} (°)	Observations (minutes)	Limiting flux density (mJy)	1FGL R_s	2FGL R_s
14	J0622.2+3751	J0621.9+3750	175.84	10.99	06:22:15	+37:51:48	0.08	0.15	0.10	32	0.10	1.07	9.34
			175.84	10.99	06:22:15	+37:51:48	0.08			10	0.18		
			175.84	10.99	06:22:15	+37:51:49	0.08			60	0.07		
			175.84	10.99	06:22:15	+37:51:49	0.08			54	0.08		
			175.84	10.99	06:22:15	+37:51:49	0.08			10	0.18		
15	J1844.2−0342c	J1844.3−0343c	28.81	−0.10	18:44:15	−03:42:46	0.04	0.08	0.08	32	0.10	9.94	9.03
			28.81	−0.10	18:44:15	−03:42:46	0.04			32	0.10		
			28.83	−0.12	18:44:22	−03:42:03	0.03			60	0.07		
			28.83	−0.12	18:44:22	−03:42:03	0.03			60	0.07		
			28.81	−0.10	18:44:15	−03:42:46	0.04			10	0.18		

SUPPORTING INFORMATION

Additional Supporting Information may be found in the online version of this article:

Table 1. Observed sources as ranked by the 2FGL logarithmic likelihood, 2FGL R_s, found through application of Gaussian-mixture modelling (Lee et al. 2012) to the 2FGL catalogue. R95 values are the major axes of the 95 per cent error ellipses for each source as found in the 1FGL and 2FGL catalogues. Limiting flux densities are calculated by the method outlined in Section 4, with a 10 per cent duty cycle imposed. Both Galactic coordinates, l and b, and equatorial coordinates, RA and Dec., show the true pointing position of each observation (http://mnras.oxfordjournals.org/lookup/suppl/doi:10.1093/mnras/sts449/-/ DC1).

Please note: Oxford University Press are not responsible for the content or functionality of any supporting materials supplied by the authors. Any queries (other than missing material) should be directed to the corresponding author for the article.

This paper has been typeset from a TEX/LATEX file prepared by the author.